Research article

Rui Feng, Laigui Hu*, Youwei Zhang, Muhammad Zaheer, Zhi-Jun Qiu*, Chunxiao Cong, Qingmiao Nie*, Yajie Qin and Ran Liu

Direct laser writing of vertical junctions in graphene oxide films for broad spectral position-sensitive detectors

https://doi.org/10.1515/nanoph-2018-0070
Received June 7, 2018; revised July 19, 2018; accepted July 19, 2018

Abstract: Heterostructures with built-in electric fields are crucial for charge separation and lateral photovoltaic effect in current position-sensitive detectors (PSDs), which have to be produced by combining semiconductors with metal or other semiconductors to form various vertical junctions (e.g. Schottky junctions) via complicated and high-cost manufacture processes. In the present work, it was found that vertical junctions can be directly written and patterned inside graphene oxide (GO) films with gradient C/O ratios by laser scribing due to the optical filter effect of the films and the formation of reduced GO (rGO) layers. Such junctions were verified to show the capability for high-precision position sensing on the micrometer scale, owing to the lateral photovoltaic effect. These self-powered laser-scribed PSDs can exhibit a small nonlinearity of <5.4%, which is far less than the acceptable level of 15%. A fast response time of about 1 ms can be obtained under a zero bias voltage, which is the fastest speed among the photodetectors based on pure rGO. Electron lateral diffusion in the upper layers of the laser-scribed devices was found to play a main role. These suggest that laser-scribed vertical junctions inside rGO are promising for high-precision displacement sensing, with the capability of low cost, flexibility, and passive operation mode.

***Corresponding authors: Laigui Hu and Zhi-Jun Qiu,** State Key Laboratory of ASIC and System, School of Information Science and Technology, Fudan University, Shanghai 200433, China, e-mail: laiguihu@fudan.edu.cn. http://orcid.org/0000-0003-1995-1423 (L. Hu); zjqiu@fudan.edu.cn (Z.-J. Qiu); and **Qingmiao Nie,** Department of Applied Physics, Zhejiang University of Technology, Hangzhou 310023, China, e-mail: nieqingmiao@zjut.edu.cn
Rui Feng, Youwei Zhang, Muhammad Zaheer, Chunxiao Cong, Yajie Qin and Ran Liu: State Key Laboratory of ASIC and System, School of Information Science and Technology, Fudan University, Shanghai 200433, China

Keywords: graphene; laser scribing; photodetectors; position-sensitive detectors; reduced graphene oxide.

1 Introduction

Position-sensitive detectors (PSDs) [1, 2], which can sense the displacement of a light spot, have been widely employed in industry, research, and military, including bridge vibration monitoring, the precision position measurement of the cantilever in atomic force microscopes, robotic vision, and guidance system [3]. In comparison to regular complex photodetector arrays for position sensing, PSDs can show relatively lower costs and higher accuracy due to the lack of interpixel discontinuity. To date, most PSDs including commercial ones are based on the expensive Si technology, in which p-n, Schottky, and p-i-n junctions [4–7] are usually used to separate excitons inside and the separated electrons/holes can diffuse laterally in the respective side of the vertical junctions, inducing the so-called lateral photovoltaic effect or a lateral photovoltage (LPV), i.e. the origin of common position sensing. A few PSDs based on organic active layers [8–11] with the advantages of easy processing, light weight, and flexibility, as well as other materials [12–15], were also demonstrated in the last decades. For organic PSDs, most of them possess a limited spectral response mainly in the visible range. Material stability and large bandgap are still the main drawbacks, although their flexibility can match well with the emerging wearable electronics.

The most advanced PSDs were recently developed using 2D materials, including monolayer graphene [16, 17] and MoS_2 [18], which can show high sensitivity and fast response time. Although Si-2D material heterojunctions were still employed to form electric fields in the devices for charge separation with Si or both materials as light absorbers, and the weak absorption of single-layer devices still limit their photoelectric conversion in the infrared (IR)

region, such works give a strong hint to use 2D materials for broad spectral high-performance PSDs with good stability. However, the related techniques, i.e. mechanical exfoliation and chemical vapor deposition, either are incompatible for massive fabrication and the emerging flexible electronics or are quite costly. Among 2D materials or their derivatives, thermally or chemically reduced graphene oxide (rGO) with a bandgap could also be a good candidate for photodetectors [19, 20] or PSDs [21] due to the capabilities of flexibility, low-cost processing, and stronger absorption even in the IR region. However, chemical rGO-based PSDs [21] exhibit poor linearity with low productivity and suffer from the difficulty of controlling the reduction process as well as residual contaminations [22].

In the present work, the low-cost transfer-free technique, i.e. laser scribing [23–27], was employed to directly "write" a 1D PSD on GO films, which was found to possess the congenital advantage for one-step time-efficient PSD fabrication due to the intrinsic optical filter effect of the films and the capability of direct patterning. GO/rGO junctions with gradient C/O ratios, which are the basis for LPV, can be directly produced in GO films. In contrast to chemical reduction, the reduction degree of rGO films can be easily controlled by laser scribing. The dependence of optoelectronic properties on the reduction degree was systematically studied. With an optimized reduction degree, self-powered PSDs with broad spectral response were fabricated. The nonlinearity of our PSDs were found to be <5.4%, which is far less than the criteria for good devices (i.e. <15%) [3]. PSDs can show power-dependent sensitivity even at a weak laser power of tens of watts, comparable to those of conventional p-i-n PSDs with bias voltages. Among pure rGO-based photodetectors, our PSDs also exhibit the fastest response time of about 1 ms. The operation principle can be addressed to the fast lateral electron diffusion in the upper rGO layers. Our results clearly indicate that vertical GO/rGO junctions for position sensing with good sensitivity can be directly written by laser scribing, which would be promising for high-precision displacement measurements with lower costs, broad spectral response, and flexibility in various optoelectronic systems.

2 Materials and methods

2.1 Device fabrication

GO nanoplatelets (XFNANO Materials Tech) with a thickness of 0.8–1.2 nm were dissolved in deionized water, and a GO dispersion with a concentration of 1.5 mg/ml was prepared after ultrasonic treatment for more than 2 h. GO films with a thickness of approximately 1 μm measured by a step profiler were acquired by drop casting on Si/SiO_2 substrates. Such films were dried in air and a drying cabinet for 1 day, respectively. Then, Au electrodes with a thickness of 80 nm were deposited by thermal evaporation through a shadow mask. The spacing between two electrodes or the length of PSDs is 100 μm. Laser reduction was carried out using a 473 nm laser (Changchun New Industries Optoelectronics Tech. Co. Ltd), whose maximum output power is 580 mW. All devices possess a strip rGO with a width of about 30 μm.

2.2 Characterization

All measurements were performed in ambient conditions. Raman spectra of GO and rGO films were obtained by a Renishaw micro-Raman spectroscopy system with a wavelength of 633 nm. Inclined cross-sectional image and C/O ratios were determined from scanning electron microscopy (SEM; Zeiss Sigma HD) with energy-dispersive spectroscopy (EDX). More thick films were used for SEM images.

Photocurrent and electrical tests were obtained using a semiconductor parameter analyzer (Agilent B1500A). Time response was collected by a digital phosphor oscilloscope (Uni-Trend Technology Ltd.). An electromagnetic shutter was used to measure the photocurrent and temporal response. All photocurrent measurements for PSDs were carried out at 0 V unless otherwise specified. Different laser sources with wavelengths of 473, 514, 633, and 1550 nm were used to measure the lateral photovoltaic effect on the motorized stage of our Renishaw Raman system under open circuit condition. Laser powers were measured by a Newport power meter 843-R.

3 Results and discussion

3.1 Laser rGO

Figure 1A is the schematic view of our laser-scribed devices and a photograph of a real device. A high-power 473 nm laser was used to reduce the solution-processed GO film with a constant sweep rate. Such GO films before laser scribing usually contain plenty of hydroxyl, epoxide, carboxyl, and carbonyl groups, as shown in the brown carbon lattice. After laser reduction, part of the oxygen-containing groups was removed (see Figure 1A, black carbon lattice). Changes can be clearly observed after

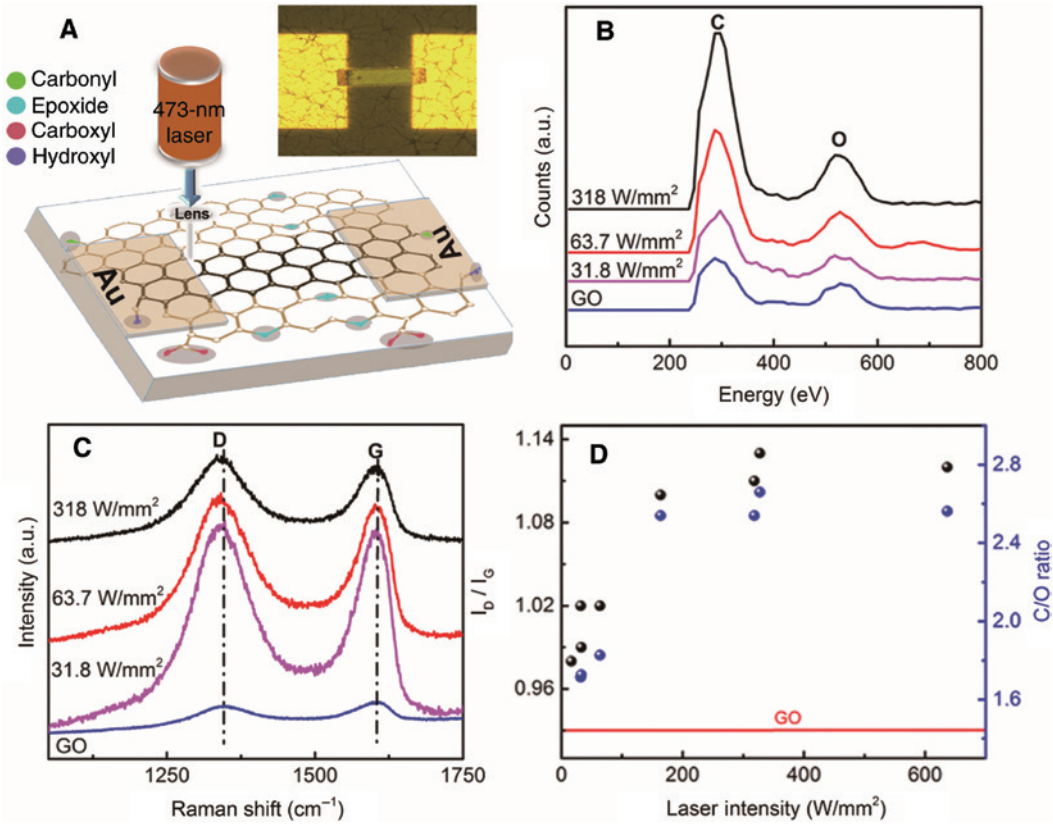

Figure 1: Characterization for laser rGO films.
(A) Schematic view of the laser-scribed devices. Brown hexagons decorated with oxygen-containing groups denote GO, whereas the black channel between two Au electrodes represents rGO. The inset is a photograph of a PSD device. (B) EDX spectra of GO and rGO films after reduction with different laser intensities. (C) Raman spectra of GO and rGO with different laser reduction intensities. (D) Dependence of I_D/I_G (black points) and C/O ratios (blue points) on the laser intensity. The red line is the I_D/I_G and C/O ratios of GO.

laser scribing from the photograph. A narrow strip of 100×30 μm² appears, which bridges the two yellow Au electrodes on GO films.

To ensure the formation of rGO, Raman spectroscopy and EDX were applied to check the reduction degree of GO films. Keeping the constant sweep rate, a C/O ratio was observed to increase with laser intensity (see Figure 1B, EDX spectra). It is natural as more energy can be absorbed for higher laser intensity to reduce the GO film with a higher degree. Figure 1C demonstrates the Raman spectra from rGO films. Two typical peaks for GO [23, 28] can be distinguished, i.e. the D band peak at 1350 cm⁻¹ attributed to structure disorder or defects and the G band peak at 1600 cm⁻¹ caused by sp² hybridization of carbon bonds. A slight red shift can be observed for both peaks when compared to the spectra of GO films (blue curve). It is notable that the D peak intensity gradually exceeds that of the G peak with the increase of laser intensity, suggesting that disorder or defect density increases with the removal of more oxygen-containing groups [29]. To demonstrate it more clearly, the ratios (I_D/I_G) between the intensities of the D and G peaks from rGO films after laser reduction with different intensities are calculated (see Figure 1D, black points). I_D/I_G ratios increase with laser intensity increasing and becoming saturated if the intensity is larger than 200 W/mm². We note that the C/O ratios (blue points) also exhibit the same tendency, suggesting that the increase of C/O ratio cannot bring about more ordered structures for the film with sp² hybridization after laser reduction. The resultant sp² clusters may still be isolated by abundant sp³ bonds in rGO. Considering that the C/O ratio obtained by EDX is an average value across the films due to a relatively large penetration depth, another possibility would be that more defects are produced as stronger laser can penetrate into the films more deeper.

3.2 C/O ratio-dependent photoresponse of rGO devices

Taking into account that the reduction degree of GO or C/O ratios will significantly influence the performance of

rGO-based photodetectors, which still lacks a systematical analysis, the reduction degree dependence of various electrical properties of rGO films was investigated to find an optimized C/O value for our devices, although the ratios obtained by EDX are average values across the films. Figure 2A shows the sheet resistance of rGO films with different C/O ratios, which was measured by a four-point probe method. The sheet resistance monotonously decreases with the increase of the ratio. The value at a ratio of ~2.4 can be estimated to be about 1.9 kΩ/sq, which was five orders of magnitude smaller than that of GO with a ratio of approximately 1.4. Hence, the enhancement induced by sp^2 hybridization dominates the conductivity increase of rGO films.

Photoresponse from rGO films was also investigated, which shows a quite different behavior from that of dark conductivity, as shown in Figure 2B. One side of the rGO device under a bias of +1 V was illuminated by the 473 nm laser (~0.05 mW) with a spot size of ~20 μm, and the other Au electrode was grounded. To avoid further reduction of the devices, low laser powers for photoresponse measurements are employed. The photocurrent of rGO devices, in which dark current has been extracted, does not show monotonous changes with the increase of C/O ratios. Maximum photoresponse can be obtained from the device with an average C/O ratio of about 2.05. Such behavior can be reproduced in more than five samples, as shown in Figure 2C in which the photocurrent was normalized to the highest value for comparison. As expected, GO devices show a negligible photoresponse (red point) due to poor light absorption and charge mobility. With the increase of C/O ratios, larger photocurrent can be generated together with the decrease of work function usually about 4.35–5.6 eV and a narrower bandgap usually about 0.5–2.2 eV [30–32]. This could be ascribed to more efficient light absorption, which induces larger photoresponse. However, the photocurrent becomes smaller after reaching a threshold average C/O value of about 2.05. Considering that more defects are generated with the increase of C/O ratios, charge trapping will become

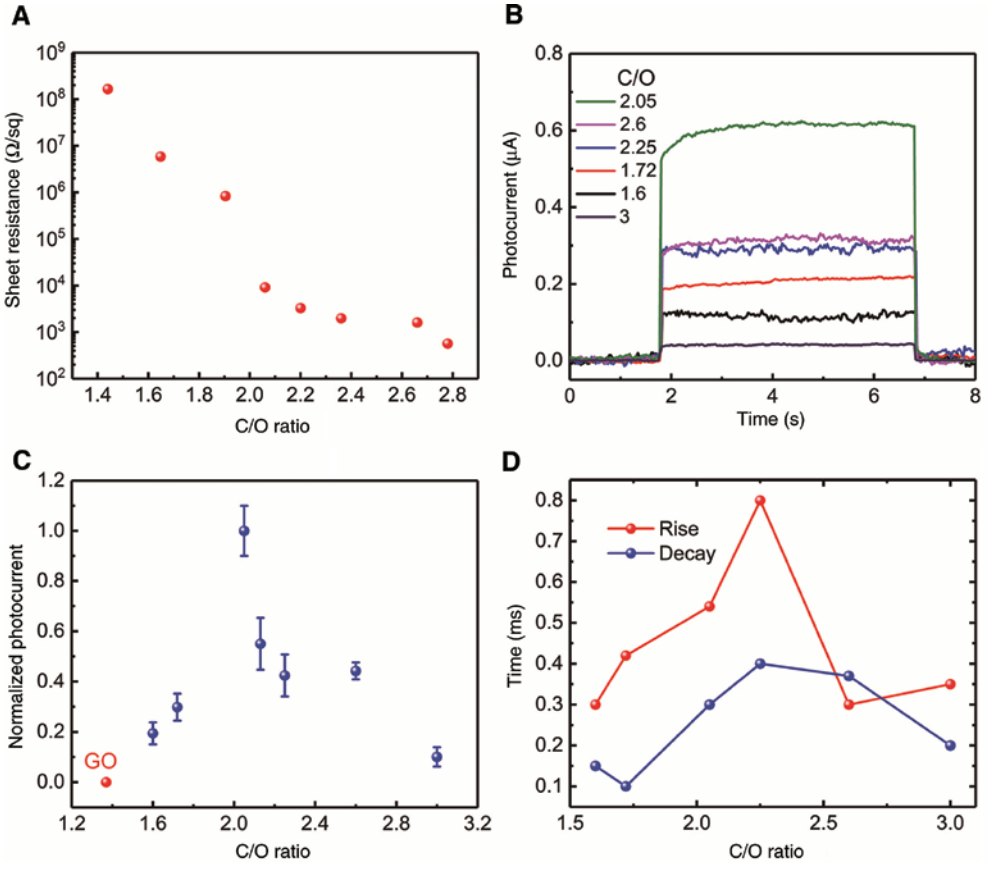

Figure 2: Impact of C/O ratio on the electrical and optoelectronic performance of rGO films.
(A) Sheet resistance as a function of C/O ratio. (B) Photoresponse of rGO devices with different C/O ratios. (C) Normalized photocurrent with error bars from rGO devices (blue points) with different C/O ratios. Negligible photocurrent can be obtained from GO devices (red point). (D) Rise (red) and decay time (blue) of rGO detectors with different C/O ratios.

more significant, inducing less free charges. Therefore, there would be a trade-off between more defects induced by oxygen removal and increased light absorption [32]. We note that the devices with a laser power (473 nm) of <2 mW do not exhibit degradation under normal operating conditions (see Supporting Information Figure S1), indicating that photochemical change or photoinduced thermal reduction in the devices is not significant. In addition, the dark current of the devices also keeps relatively stable in air even after 30 days, suggesting that oxygen- or moisture-induced changes in rGO films without sealing are negligible.

Rise (10–90%; red points) and decay time (90–10%; blue points) [33] of the devices with different C/O ratios were also investigated by an oscilloscope, as shown in Figure 2D. A similar trend with that of photocurrent was obtained. However, the device with an average ratio of 2.25 exhibits the longest response time with the rise time of 0.8 ms and decay time of 0.4 ms, respectively, which are the fastest values to date for pure rGO-based photodetectors [20, 34–36]. The longer response time with the increase of C/O ratio (<2.25) matches well with the fact that the trapping/detrapping effect due to more defects or lattice disorder is significant. However, decreased response time is observed at ratios of >2.25. These could be ascribed to the fact that the upper layers are closer to ideal graphene layers with decreased defects due to the annealing effect with a stronger laser, although more defects are still produced in the bottom layers, owing to a deeper laser penetration.

3.3 Position-dependent photoresponse of rGO devices

The photoresponse at other positions of rGO films with different C/O ratios was also collected under a bias of 1 V at 473 nm (200 μW), as shown in Figure 3, in which the zero point denotes the central point of the devices. It is notable that the rGO device with the average C/O ratio of 2.05 still demonstrates the largest photocurrent with the laser spot at other positions away from the central point (see Figure 3A). The photocurrent clearly exhibits a dependence on the position of laser spots. We note that the positions close to the two electrodes demonstrate the largest photocurrent with opposite polarities. However, the laser spot at the central point produces the smallest photocurrent. Figure 3B and C shows the wavelength and power dependences of the photoresponse at different positions, respectively. For comparison, responsivity R is calculated for each wavelength based on the relation $R = I_{ph}/P_{in}$, where I_{ph} is the photocurrent and P_{in} is the incident light power. A broad spectral response was observed for rGO devices, which covers the IR wavelength of 1550 nm in spite of a smaller responsivity (see Figure 3B). All photoresponses with different laser wavelengths exhibit the similar trend as well as those in Figure 3C with different laser powers (633 nm). We note that the photocurrent increases with the increase of laser powers at the regions away from the central point. Therefore, the position-dependent photoresponse does not show dependence on a certain laser power and wavelength. In addition, the relationship between light power and the photocurrent obeys a power law and exhibits quasi-linearity (see Supporting Information Figure S2).

3.4 PSDs

Considering that laser scribing may induce the inhomogeneous reduction of GO across a thick film due to the optical filter effect of upper layers or a finite penetration length of laser beams, gradient rGO/GO junctions could be produced in which vertical built-in electric

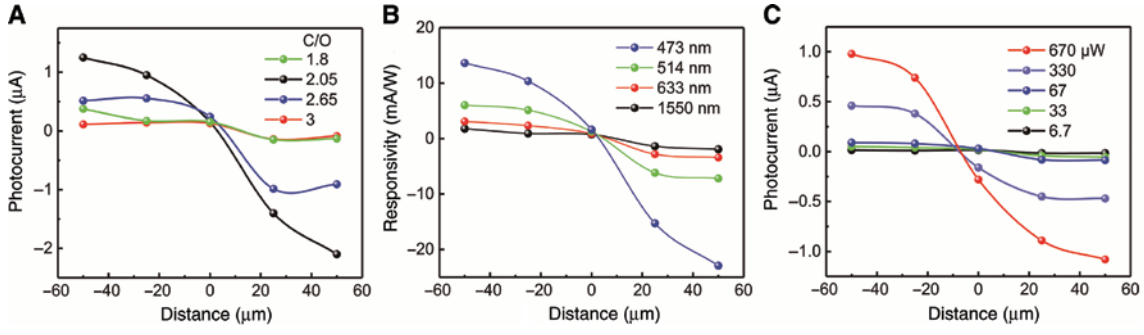

Figure 3: Photoresponse of rGO films at different positions of laser spots with (A) different C/O ratios (473 nm laser), (B) different laser wavelengths, and (C) different laser powers at 633 nm.

fields can be generated for charge separation and LPV. Position-dependent photovoltage was demonstrated for our rGO devices with the optimized C/O ratio under open circuit condition without a bias voltage. Figure 4A shows the LPVs of an rGO device at different positions x. For the positions below the Au electrodes (colored areas), LPV decreases with the increase of the distance. However, the self-powered device exhibits a linear relationship between the LPV and the position of laser spot (633 nm, 670 μW) in the channel, which can be explained by the carrier diffusion theory [18, 37]. For $-L<x<L$, LPV can be expressed as follows:

$$\mathrm{LPV} = KN_0[\exp(-(L-x)/l) - \exp(-(x+L)/l)], \quad (1)$$

where K is the proportionality coefficient and N_0 is the density of excess charges at x. L and l denote the half-distance of the gap between the electrodes and the charge diffusion length in rGO, respectively. If $x<<l$, Eq. (1) can be simplified as

$$\mathrm{LPV} = (2KN_0/l)\exp(-L/l)x = ax, \quad (2)$$

where slope a is usually defined as the sensitivity for PSDs, representing the displacement resolution of PSDs. Therefore, the linear relationship can be ascribed to a large l when compared to x in the devices. Based on Equations (1) and (2) with the data in Figure 4A, l can be estimated to be about 62.2 μm, which is much larger than x and naturally induces the linearity. In addition, the photocurrent from the device without applying a bias voltage also exhibits linearity (see Supporting Information Figure S3), suggesting that the nonlinearity in Figure 3 can be ascribed to the applied bias voltage.

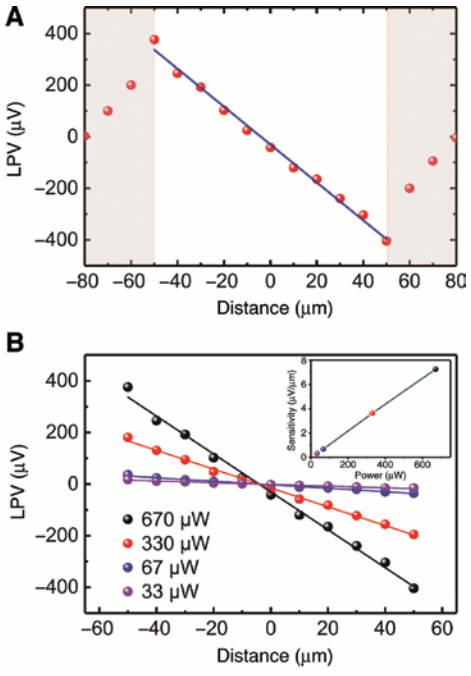

Figure 4: Lateral photovoltaic effect for the laser-scribed rGO devices: (A) LPV at different positions of laser spots (633 nm) and (B) LPV between the two Au electrodes with different laser powers. The inset is the sensitivity at different laser powers.

It is notable that LPV-distance curves with different laser powers also keep the linearity, as shown in Figure 4B, in spite of different slope values (i.e. the sensitivity). The sensitivity increases with the increase of the laser powers linearly (see inset), ranging from 0.33 to 7.27 μV/μm with the laser power increasing from 33 to 670 μW. Therefore, higher sensitivity can be expected if a larger laser power is used. It is natural as a larger N_0 can be produced for higher laser powers, leading to a larger sensitivity. Another parameter used to evaluate the signal distortion of PSDs, i.e. nonlinearity, was estimated based on the following equation [3, 38]:

$$\text{Nonlinearity} = 2\times\text{RMS deviation/Measured full scale} \quad (3)$$

The maximal nonlinearity in Figure 4B can be calculated to be 5.4%, which is far less than the acceptable criteria of 15% for PSDs. In addition, rise and decay time for the self-powered PSDs were also estimated to be about 1.6 and 1.9 ms, respectively (see Supporting Information Figure S4A). It is notable that the response speed of our PSDs does not show significant dependence of the position of laser spots (see Supporting Information Figure S4B). To our best knowledge, these values are still the fastest response among pure rGO-based devices even with bias voltages. This could be ascribed to a smaller amount of defects in the upper layers of our rGO films and a short carrier transit distance, considering the longer response time of about 10 s in chemical rGO films with a similar channel distance [34].

3.5 Mechanisms for laser-scribed PSDs

Inclined cross-sectional SEM image with EDX spectra of a laser rGO film was collected to verify the existence of possible junctions (see Figure 5A). As we expected, the C/O ratios of rGO films gradually decrease from the film surface (point 1) with a value of 2.4 to the bottom (point 3) with a value of 1.54. The value at the middle point 2 is about 2.16. Hence, a gradient junction across rGO films should exist (see the energy alignment of the films in Figure 5B). Taking into account that rGO films are usually p-type semiconductors and the work function will gradually decrease

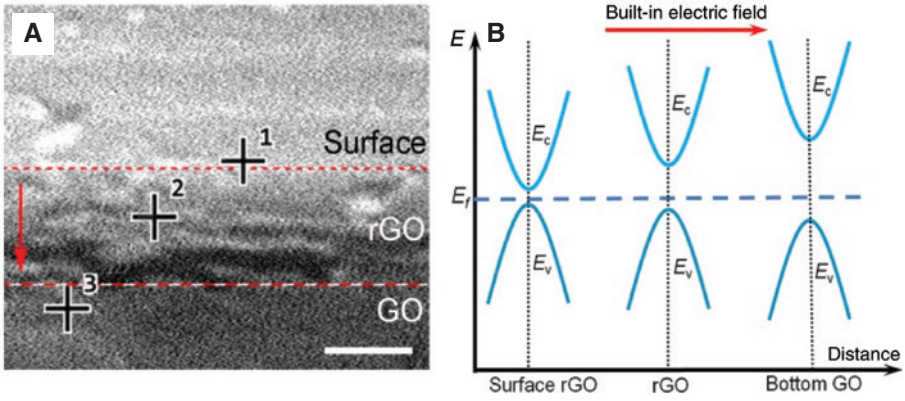

Figure 5: Gradient C/O ratios in the laser-scribed rGO films.
(A) Inclined cross-sectional SEM image of a thick rGO film. The scale bar is 1 μm, The ratios at points 1–3 can be determined by EDX.
(B) Scheme of the energy alignment across the rGO film, in which E_c and E_v are conduction and valence bands, respectively. E_f denotes the Fermi level. Red arrows denote the built-in electric field in the junctions.

with the increase of C/O ratios and a narrower bandgap, the gradient C/O ratio in rGO films will induce built-in electric fields from the upper layers toward the bottom layers, as shown in Figure 5 (red arrows). Upon light illumination, photogenerated excitons can be separated by the fields with electrons in the upper layers and holes in the bottom layers. The excess electrons in the upper rGO films can laterally diffuse to both sides of the devices, producing a lateral potential difference between illuminated and nonilluminated areas with an electron density gradient. The difference of collected electron quantity by the two electrodes thus induces the LPV.

To further confirm the role of laser-scribed junctions for PSDs, thermal rGO devices with the same device structure were investigated for comparison (see Supporting Information Figure S5). It was noted that the thermally reduced films nearly exhibit a uniform reduction degree. The same laser used in Figure 4A with a light power of 670 μW was employed to study their LPV. We note that LPV from rGO films does not exhibit significant C/O ratio dependence. The signals are very weak and >16 times smaller than those from the laser-scribed devices. In addition, weak LPV does not show good linearity. These clearly indicate that LPV is mainly caused by the laser-scribed junctions as well as charge diffusion in rGO-based PSDs.

4 Conclusions

In summary, vertical junctions were directly written inside GO films by laser scribing, which can be employed for position sensing. It exhibits high priority to manufacture PSDs by this one-step technique with lower cost and short time consumption. Due to the optical filter effect of upper rGO layers during laser scribing, gradient C/O ratios across the laser-scribed rGO films can be easily generated, inducing junctions inside the devices with built-in electric fields for exciton dissociation as well as LPV. Such rGO-based PSDs with optimized C/O ratios can show broad spectral response from visible to IR region and a sensitivity of 7.27 μV/μm with a spatial resolution of meter scale. Higher sensitivity can be expected due to the linear relationship between laser power and sensitivity. The nonlinearity for these PSDs is found to be <5.4%, which is much smaller than the usual acceptable level of 15%. In addition, our self-powered devices can exhibit the highest response time of about 1 ms among pure rGO-based photodetectors. These possess significant implication on the application of laser-scribed rGO with vertical junctions for high-precision displacement sensing.

Acknowledgments: This work was supported by the Key Program of Natural Science Foundation (No. LZ13F050002) of Zhejiang Province, the Shanghai Pujiang Program (No. 16PJ1401000), the Natural Science Foundation of Shanghai (Nos. 17ZR1446600, 17ZR1446500, and 16ZR1402500), the National Natural Science Foundation of China (Nos. 61774042 and 61774040), and the "First-Class Construction" project of Fudan University.

References

[1] Contreras J, Martins R, Wojcik P, et al. Color sensing ability of an amorphous silicon position sensitive detector array system. Sensor Actuat A Phys 2014;205:26–37.
[2] Sui JX, Zhang X. Vibration measurement system based on position sensitive detector. Sensor Rev 2011;31:120–6.

[3] Henry J, Livingstone J. Thin-film amorphous silicon position-sensitive detectors. Adv Mater 2001;13:1023–6.
[4] Fortunato E, Lavareda G, Vieira M, Martins R. Thin-film position-sensitive detector based on amorphous-silicon p-i-n-diode. Rev Sci Instrum 1994;65:3784–6.
[5] Fortunato E, Lavareda G, Martins R, Soares F, Fernandes L. Large-area 1D thin-film position-sensitive detector with high detection resolution. Sensor Actuat A Phys 1995;51:135–42.
[6] Martins R, Teodoro P, Soares F, et al. Application of amorphous silicon thin-film position-sensitive detector to optical rules. Adv Eng Mater 2001;3:174–7.
[7] Cabrita A, Figueiredo J, Pereira L, et al. Thin film position sensitive detectors based on pin amorphous silicon carbide structures. Appl Surf Sci 2001;184:443–7.
[8] Kabra D, Singh TB, Narayan KS. Semiconducting-polymer-based position-sensitive detectors. Appl Phys Lett 2004;85:5073–5.
[9] Koeppe R, Bartu P, Bauer S, Sariciftci NS. Light- and touch-point localization using flexible large area organic photodiodes and elastomer waveguides. Adv Mater 2009;21:3510–4.
[10] Cabanillas-Gonzalez J, Pena-Rodriguez O, Lopez IS, et al. Organic position sensitive photodetectors based on lateral donor-acceptor concentration gradients. Appl Phys Lett 2011;99:103305.
[11] Arndt AP, Kettlitz SW, Mescher J, Lemmer U. Position sensing by transient photocurrents of organic photodiodes. IEEE Photonic Tech L 2016;28:617–20.
[12] Lan TA, Liu SA, Wang H. Enhanced lateral photovoltaic effect observed in CdSe quantum dots embedded structure of Zn/CdSe/Si. Opt Lett 2011;36:25–7.
[13] Liu S, Wang H, Yao YJ, Chen L, Wang ZL. Lateral photovoltaic effect observed in nano Au film covered two-dimensional colloidal crystals. Appl Phys Lett 2014;104:111110.
[14] Ashar AZ, Ganesh N, Narayan KS. Hybrid perovskite-based position-sensitive detectors. Adv Electron Mater 2018;4:1700362.
[15] St-Antoine BC, Menard D, Martel R. Position sensitive photothermoelectric effect in suspended single-walled carbon nanotube films. Nano Lett 2009;9:3503–8.
[16] Wang WH, Du RX, Guo XT, et al. Interfacial amplification for graphene-based position-sensitive-detectors. Light Sci Appl 2017;6:e17113.
[17] Wang WH, Yan ZZ, Zhang JF, Lu JP, Qin H, Ni ZH. High-performance position-sensitive detector based on graphene-silicon heterojunction. Optica 2018;5:27–31.
[18] Cong RD, Qiao S, Liu JH, et al. Ultrahigh, ultrafast, and self-powered visible-near-infrared optical position-sensitive detector based on a CVD-prepared vertically standing few-layer MoS_2/Si heterojunction. Adv Sci 2018;5:1700502.
[19] Zhu M, Li XM, Guo YB, et al. Vertical junction photodetectors based on reduced graphene oxide/silicon Schottky diodes. Nanoscale 2014;6:4909–14.
[20] Alsaedi D, Irannejad M, Ibrahim KH, Almutairi A, Ramahi O, Yavuz M. High-responsivity reduced graphene oxide gel photodetectors for visible-light detection with a large detection area and an end-contact interface. J Mater Chem C 2017;5:882–8.
[21] Moon IK, Ki B, Yoon S, Choi J, Oh J. Lateral photovoltaic effect in flexible free-standing reduced graphene oxide film for self-powered position-sensitive detection. Sci Rep 2016;6:33525.
[22] Abdelsayed V, Moussa S, Hassan HM, Aluri HS, Collinson MM, Elshall MS. Photothermal deoxygenation of graphite oxide with laser excitation in solution and graphene-aided increase in water temperature. J Phys Chem Lett 2010;1:283–98.
[23] Wang X, Tian H, Mohammad MA, et al. A spectrally tunable all-graphene-based flexible field-effect light-emitting device. Nat Commun 2015;6:7767.
[24] El-Kady MF, Strong V, Dubin S, Kaner RB. Laser scribing of high-performance and flexible graphene-based electrochemical capacitors. Science 2012;335:1326–30.
[25] Kumar R, Singh RK, Singh DP, Joanni E, Yadav RM, Moshkalev SA. Laser-assisted synthesis, reduction and micro-patterning of graphene: recent progress and applications. Coord Chem Rev 2017;342:34–79.
[26] Feng R, Zhang Y, Hu L, et al. Laser-scribed highly responsive infrared detectors with semi-reduced graphene oxide. Appl Phys Express 2018;11:015101.
[27] Zhang YL, Guo L, Wei S, et al. Direct imprinting of microcircuits on graphene oxides film by femtosecond laser reduction. Nano Today 2010;5:15–20.
[28] Strong V, Dubin S, El-Kady MF, et al. Patterning and electronic tuning of laser scribed graphene for flexible all-carbon devices. ACS Nano 2012;6:1395–403.
[29] Moon IK, Lee J, Ruoff RS, Lee H. Reduced graphene oxide by chemical graphitization. Nat Commun 2010;1:73.
[30] Kumar PV, Bernardi M, Grossman JC. The impact of functionalization on the stability, work function, and photoluminescence of reduced graphene oxide. ACS Nano 2013;7:1638–45.
[31] Guo L, Shao RQ, Zhang YL, et al. Bandgap tailoring and synchronous microdevices patterning of graphene oxides. J Phys Chem C 2012;116:3594–9.
[32] Chang H, Sun Z, Yuan Q, et al. Thin film field-effect phototransistors from bandgap-tunable, solution-processed, few-layer reduced graphene oxide films. Adv Mater 2010;22:4872–6.
[33] Cao Y, Yang H, Zhao Y, et al. Fully suspended reduced graphene oxide photodetector with annealing temperature-dependent broad spectral binary photoresponses. ACS Photonics 2017;4:2797–806.
[34] Chitara B, Panchakarla L, Krupanidhi S, Rao C. Infrared photodetectors based on reduced graphene oxide and graphene nanoribbons. Adv Mater 2011;23:5419–24.
[35] Li G, Liu L, Wu G, et al. Self-powered UV-near infrared photodetector based on reduced graphene oxide/n-Si vertical heterojunction. Small 2016;12:5019–26.
[36] Ghosh S, Sarker BK, Chunder A, Zhai L, Khondaker SI. Position dependent photodetector from large area reduced graphene oxide thin films. Appl Phys Lett 2010;96:163109.
[37] Yu CQ, Wang H, Xia YX. Enhanced lateral photovoltaic effect in an improved oxide-metal-semiconductor structure of TiO_2/Ti/Si. Appl Phys Lett 2009;95:1022.
[38] Yu CQ, Wang H, Xiao SQ, Xia YX. Direct observation of lateral photovoltaic effect in nano-metal-films. Opt Express 2009;17:21712–22.

Supplementary Material: The online version of this article offers supplementary material (https://doi.org/10.1515/nanoph-2018-0070).